

Chapter 7

Application of DAS to Inorganic Salts

Dynamic-angle spinning has proven quite valuable in the evaluation of the electric field gradients present at the nuclei in a variety of inorganic salts. Specifically, the alkali metals are particularly conducive for study with NMR. All of these nuclei are spin-3/2 and possess a manageable quadrupolar moment. In the case of ${}^7\text{Li}$ and ${}^{133}\text{Cs}$, the quadrupolar interactions are generally small enough that MAS is sufficient to achieve high resolution spectra. The nuclei of ${}^{87}\text{Rb}$, ${}^{85}\text{Rb}$ and ${}^{23}\text{Na}$, however, require the more complete averaging of a technique like DAS or DOR.

Sodium

This nucleus was one of the first evaluated with DAS. The large gyromagnetic ratio and high natural abundance make this a natural candidate for study with DAS. However, these two factors conspire to make the homonuclear dipolar interaction quite strong and therefore highest resolution is only achieved in samples where the sodium is magnetically diluted, for example in crown ether complexes or with bulky anions in ionic salts. Unfortunately, the total chemical shift range for this nucleus is quite small, as is the range of electric field gradients, since this is a fairly small cation. Therefore, the overall linewidth from the homonuclear dipolar coupling (see chapter 3) renders DAS insensitive to small variations in the local EFG and chemical shift interaction. Examples of sodium spectra are shown in both chapter 3 and chapter 5.

Rubidium Salts

The application of dynamic-angles spinning NMR has also been extended to other inorganic salts.⁵⁴ Specifically, ${}^{87}\text{Rb}$ has proven to be an extremely sensitive nucleus for DAS experiments. ${}^{87}\text{Rb}$ and alkali metals in general are important in a number of areas,

they serve as promoters in catalysts, for example, the heterogeneous catalysis of ammonia synthesis¹²⁴ and oxidative coupling of methane to yield ethane and ethene.¹²⁵ Rubidium is an important component of some glasses,¹²⁶ and recently, it has been shown that Buckminsterfullerene, C₆₀, doped with Rb metal becomes superconducting at 28 K.¹²⁷

In order to assess the applicability of DAS to rubidium and its potential to yield structural information about materials such as those listed above, ⁸⁷Rb MAS, VAS and DAS spectra of five inorganic salts were obtained. The salts chosen were RbCl, RbClO₄, Rb₂SO₄, Rb₂CrO₄ and RbNO₃ because they had been previously studied with static NMR experiments^{128,129} and the crystal structures were well known.¹³⁰⁻¹³⁵

In the study by Cheng *et al.*,¹²⁸ the T_1 relaxation times for each of these salts was measured and all were between 100 and 300 ms. We performed the VAS, MAS, and DAS experiments using a probe designed by Mueller *et al.*⁵¹ We used the usual DAS pulse sequences (see chapters 3 and 4) for both the 1D spectra⁴² and for the pure-phase MAS detected spectra.⁵⁰ Our central transition selective 90° pulses were between 4.0 and 6.0 μ s. Our hopping times were usually between 30 and 50 ms and our data sets were 128 t_1 points by 512 complex t_2 points. All MAS and variable-angle spinning (VAS) spectra were acquired with a standard Hahn-echo pulse sequence ($\pi/2 - n t_r - \pi - t_{rd} - \text{acquire}$) where t_r is the rotor period, n is an integer and $n t_r$ was between 500 and 1500 μ s. The t_{rd} delay was used to allow collection of the whole echo.

For ⁸⁷Rb, as with all quadrupolar nuclei, the measured isotropic shift in DAS has a field dependence because it is the sum of two contributions.

$$\delta_{obs} = \delta_{isacs} + \delta_{iso}^{(2Q)} \quad (7.1)$$

These two terms are the isotropic chemical shift and the isotropic second-order quadrupolar shift, respectively. The isotropic chemical shift is field independent when expressed in units of ppm while the second-order quadrupolar shift has a strong field dependence given below.

$$\delta_{iso}^{(2)} = -\frac{3 \times 10^6}{40} \frac{C_Q^2 \left(I(I+1) - \frac{3}{4} \right) \left(1 + \frac{\eta_Q^2}{3} \right)}{\omega_I^2 I^2 (2I-1)^2} \quad (7.2)$$

All constants have their usual meanings. Using equations 7.1 and 7.2, we may calculate isotropic chemical shifts by measuring isotropic shifts at two field strengths. To do this, we solve the system of linear equations from equation 7.3 evaluated at two B_0 fields. Equation 7.3 (the reduced version of equation 7.1) may be expressed as follows for ^{87}Rb in units of ppm.

$$\begin{aligned} \delta_{obs} &= \delta_{isacs} - \left(1.28 \times 10^{-10} \frac{\text{T}^2}{\text{Hz}^2} \right) C_Q^2 \left(1 + \frac{\eta_Q^2}{3} \right) \frac{1}{B_0^2} \\ &= \delta_{isacs} - \left(1.28 \times 10^{-10} \frac{\text{T}^2}{\text{Hz}^2} \right) P_Q^2 \frac{1}{B_0^2} \\ P_Q &= C_Q \sqrt{1 + \frac{\eta_Q^2}{3}} \end{aligned} \quad (7.3)$$

It is important to note that it is impossible to extract the C_Q from η_Q using only multiple field experimental 1D DAS results. However, multiple field results do help to minimize experimental error in the final results.

Figure 7.1 shows the ^{87}Rb VAS spectra and the angles of acquisition. Only the RbCl is clearly resolved. This is because of the absence of quadrupolar coupling due to the cubic crystal structure of RbCl. Figures 7.2 and 7.3 show the DAS spectra at 11.7T and 9.4T respectively. There is an order of magnitude narrowing of the DAS spectra compared to the VAS spectra. In the cases where multiple lines are present due to spinning sidebands, the isotropic peaks were identified by spinning at multiple spinning rates.

The VAS spectra in figure 7.1 show the resolving power of simple one-dimensional NMR techniques applied to Rb salts. In all cases except RbNO₃ and Rb₂CrO₄, the individual sites are clearly separated. However, only the RbCl spectrum yields a single narrow line which may be used to measure the isotropic shift. The other spectra would all require simulations to extract the actual isotropic shifts, and in the case of RbNO₃, the simulation would be quite difficult due to the extreme overlap of the three sites.

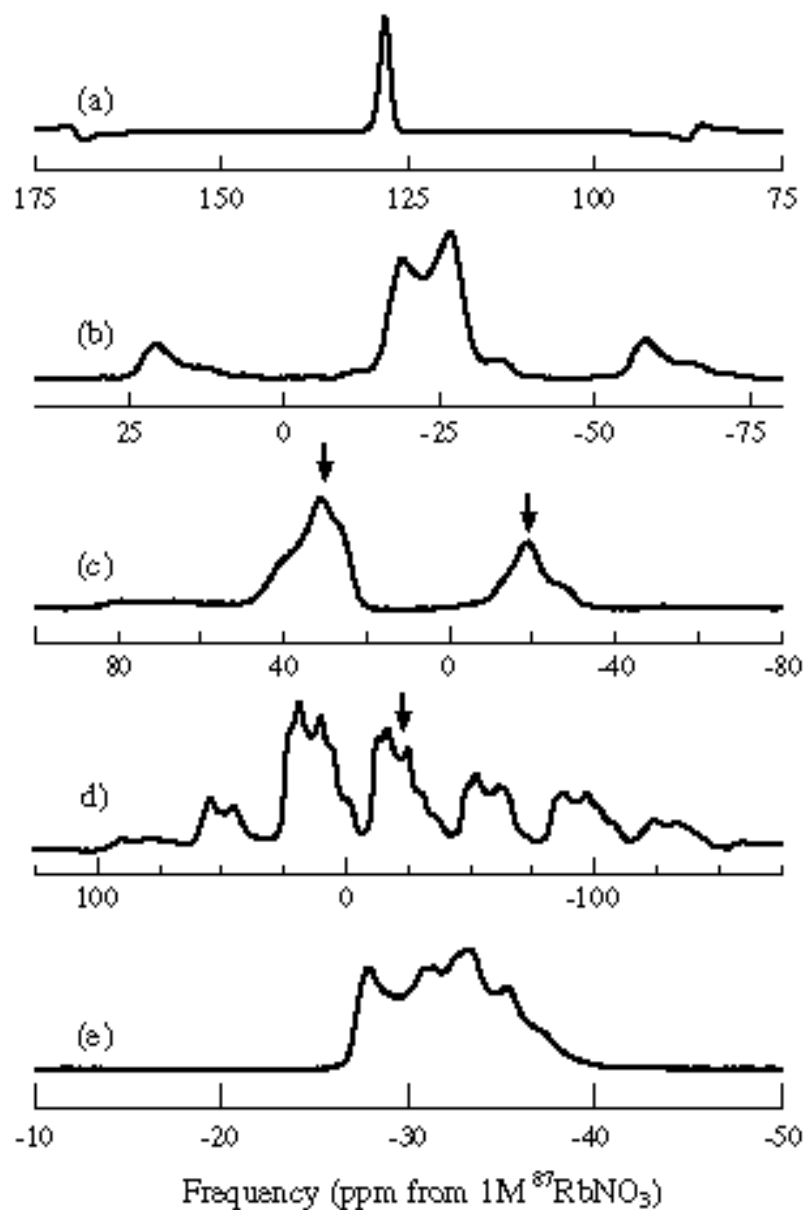


Figure 7.1 ^{87}Rb Salts 11.7T VAS Spectra. (a) RbCl at 54.74° , (b) RbClO_4 at 54.74° , (c) Rb_2SO_4 at 79.19° , (d) Rb_2CrO_4 at 54.74° , (e) RbNO_3 at 54.74° .

The DAS spectra at 11.7T reveal the actual isotropic shifts for each site in each compound (except the broadest site in Rb_2CrO_4) without the need for simulations. This has the advantage of greatly improving the accuracy of the measurement of the isotropic shifts. In the case of Rb_2SO_4 , the DAS spectrum illustrates one of the classic problems with VAS spectra.

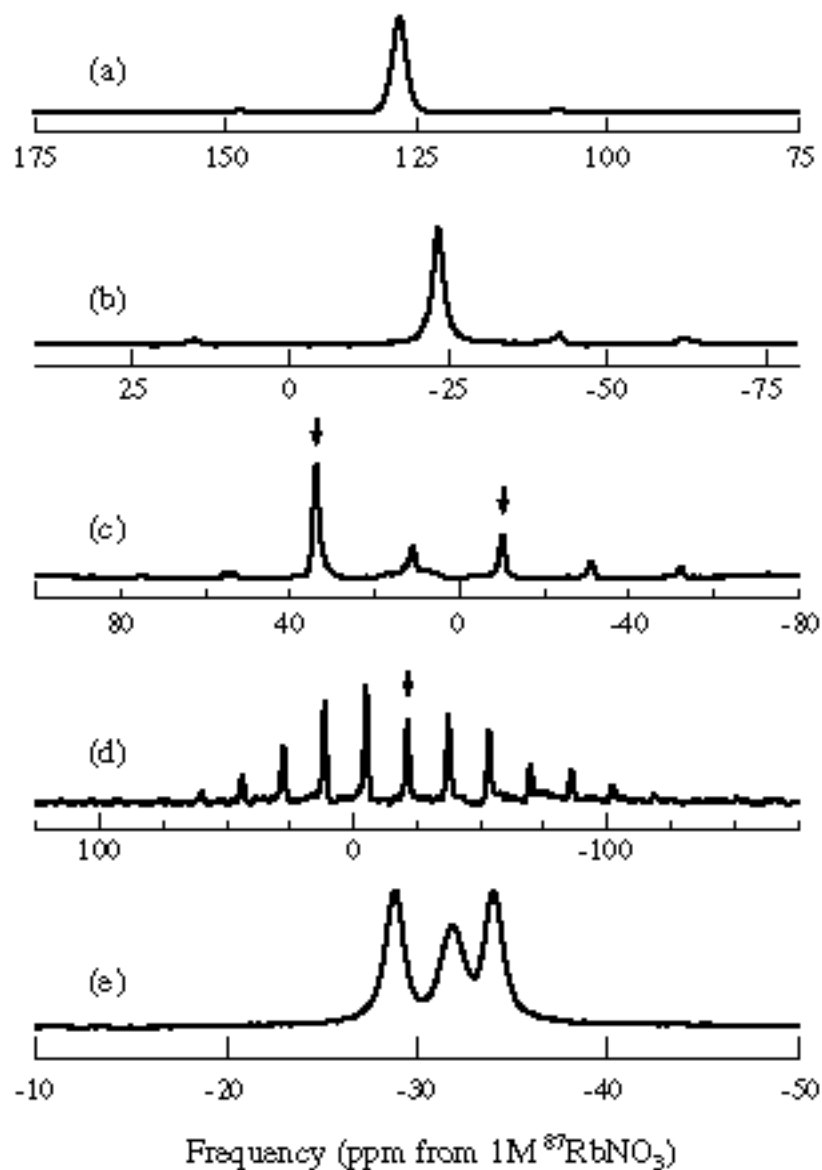


Figure 7.2 ^{87}Rb Salts 11.7T DAS Spectra. (a) RbCl , (b) RbClO_4 , (c) Rb_2SO_4 , (d) Rb_2CrO_4 , (e) RbNO_3 .

The actual isotropic shifts in this salt (as seen in the DAS spectrum, figure 7.2c) do not correspond to the highest point in the VAS spectrum (figure 7.1c), rather, the isotropic shifts in the VAS spectrum fall at the overall centers of gravity of each peak. Low intensity contributions in the wings of the VAS peaks make calculation of the center of gravity of these peaks difficult.

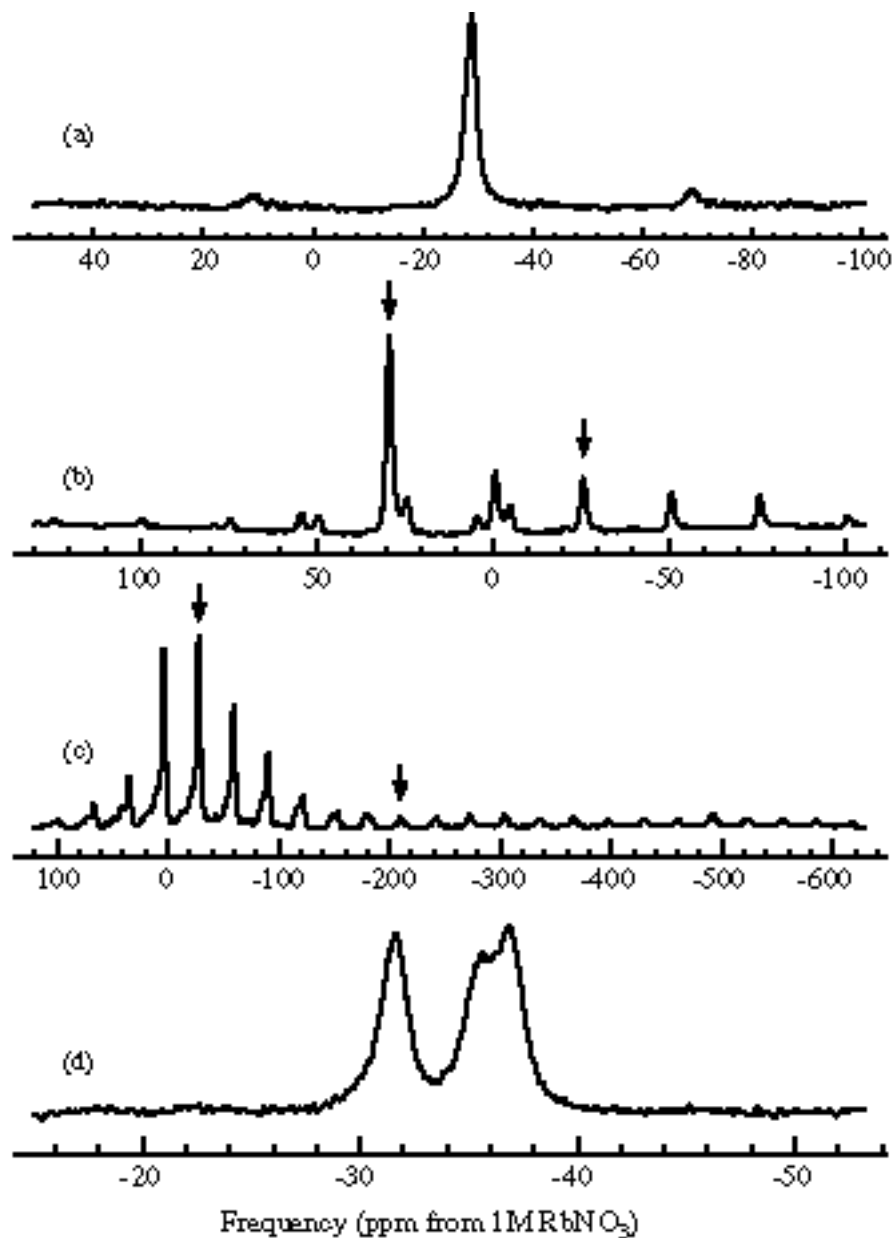


Figure 7.3 ^{87}Rb Salts 9.4T DAS Spectra. (a) RbClO_4 , (b) Rb_2SO_4 , (c) Rb_2CrO_4 , (d) RbNO_3 .

Figure 7.3 shows the DAS spectra of the same salts at a lower field strength. Notice that the spectra all have the same high resolution of the 11.7T spectra in figure 7.2. However, now some of the peaks fall at different isotropic positions because of differences in the second order quadrupolar isotropic shifts (see equation 7.2 and 7.3). The cubic RbCl does not shift at all, since this salt has zero electric field gradients at the Rb nucleus (as evidenced earlier by the narrow MAS spectrum in figure 7.1a). All other

peaks shift slightly down field to more negative ppm values. Also, the number of spinning sidebands for a given site differs between the two fields, due to the fact that the overall size of the second-order broadening (which appears in the expressions for sideband intensities in chapter 3) is increased at lower field. Also, since the chemical shift scales with the field, the CSA contribution to the sidebands will actually be reduced at the lower field (this is the reason much of the ^{13}C and ^{31}P MAS NMR work is done at lower field strengths).

Compound	$^{9.4T}_{obs}$ (ppm)	$^{11.7T}_{obs}$ (ppm)	$^{(CS)}_{iso}$ (ppm)	P_Q (MHz)
RbCl	127±1	127±1	127±2	0
RbClO ₄	-28±1	-23±1	-14±2	3.1±0.3
Rb ₂ SO ₄	-25±1	-10±1	16±2	5.3±0.2
	29±1	34±1	42±2	3.0±0.3
Rb ₂ CrO ₄	-27±1	-21±1	-11±2	3.3±0.3
	-201±2	a	a	a
RbNO ₃	-32±1	-29±1	-24±2	2.4±0.4
	-36±1	-32±1	-25±2	2.8±0.4
	-37±1	-34±1	-29±2	2.4±0.4

Table 7.1 ^{87}Rb Isotropic Shifts and Coupling Products. The isotropic chemical shifts and quadrupolar products were calculated using equation 7.3. ^aThis site was too broad for detection at 11.7T with both the DAS and MAS experiments.

In the case of Rb₂CrO₄, the second broad site at -201 ppm appears in the 9.4 T spectrum which was absent in the higher field spectrum. Also, the overall number of sidebands around the -27 ppm peak is greatly reduced at 9.4 T, since the major contribution to the anisotropic broadening of this site is the chemical shift interaction. This actually may be seen in the MAS spectrum (figure 7.1d) where the individual sidebands have clearly resolved quadrupolar MAS patterns. Normally, when large numbers of sidebands result from quadrupolar coupling alone, the MAS pattern will be greatly distorted and overlap-

ping with the sidebands. In the case of Rb_2CrO_4 , this is not observed, showing that the CSA is quite large for this site. All of the measured isotropic shifts are compiled in table 7.1 below.

The two field DAS measurements were used to generate both the quadrupolar coupling products and isotropic chemical shifts for these salts using equation 7.3. These values are tabulated in table 7.1. The values of the quadrupolar products and isotropic shifts in table 7.1 may now be compared to the values arrived at by Cheng *et al.*¹²⁸ from static simulations compiled in table 7.2. For the case of the RbCl , our results agree exactly with those of Cheng *et al.*¹²⁸

Compound	$^{(CS)}_{iso}$ (ppm)	η_Q	P_Q (MHz)
RbCl	128.0	0	0
RbClO_4	3.8	0.16	3.2
Rb_2SO_4	3.0	0.13	3.2
	46.6	0.89	2.9
Rb_2CrO_4	-47.4	0.48	5.4
	52.8	0.75	12.5
RbNO_3	*	*	*

Table 7.2 Previously Measured ^{87}Rb Isotropic Chemical Shifts and Quadrupolar Parameters. These parameters were determined by simulating static central transition multi-site patterns with both quadrupolar and chemical shift anisotropy parameters by Cheng *et al.* For RbNO_3 , the three sites could not be resolved.

For other compounds, the agreement is much worse, indicating the difficulty of relying only on static simulations (which have a large number of parameters to adjust) in measuring quadrupolar and chemical shift parameters. The rough size of the coupling constants measured by Cheng *et al.*¹²⁸ for the RbClO_4 and Rb_2CrO_4 are in the correct range. However, in all cases except for RbCl , the isotropic chemical shifts are quite inaccurate. Also, in the case of RbNO_3 , which has the strongest overlap, the static simulations fail completely.

Improvements from Multiple-Field DAS

To improve the overall accuracy and precision for the measurement of the isotropic chemical shifts and quadrupolar coupling products, the DAS measurement should be made at more than two fields. In this case, the system of equations which relate the measured isotropic shifts to the isotropic chemical shift and second-order quadrupolar coupling products are over-determined.

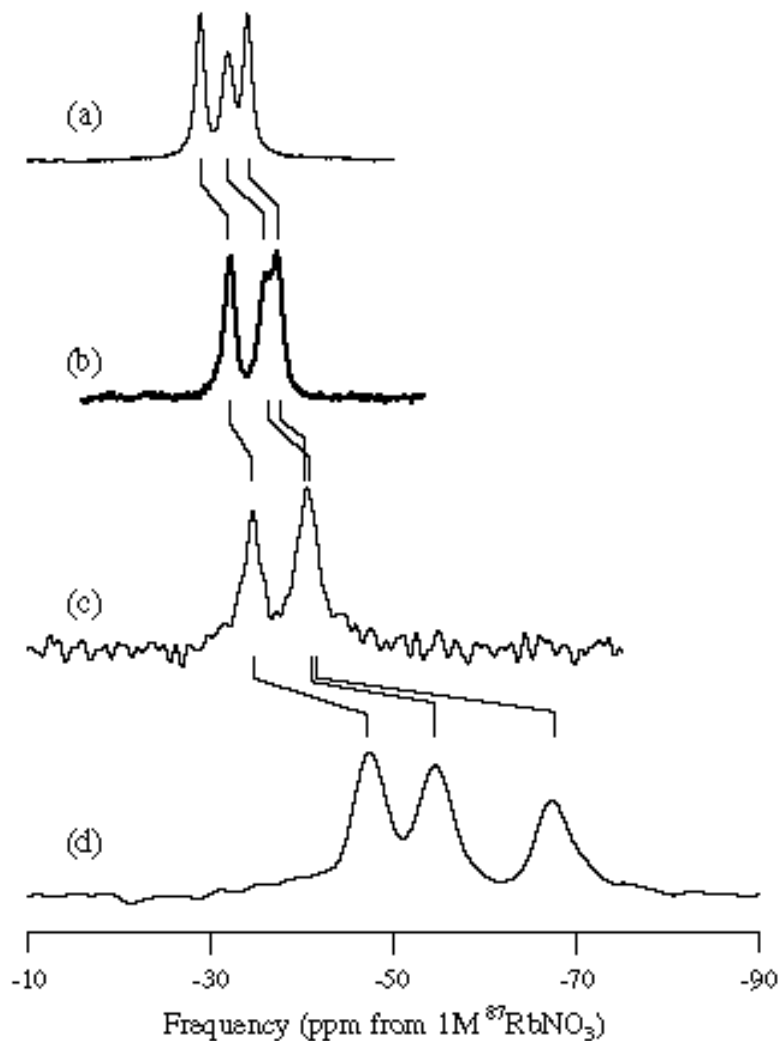


Figure 7.4 RbNO₃ Spectra at Four Field Strengths. (a) 11.7T, (b) 9.4T, (c) 7.0T and (d) 4.2T.

This opens the possibility of a linear least-squares fit of the isotropic shifts when plotted versus the reciprocal of the field strength squared. Figure 7.4 shows the RbNO₃ spectra measured at 11.7 T (a), 9.4 T (b), 7.0 T (c) and 4.2 T (d). Notice in figure 7.4 that the

overall resolution in ppm seems to get worse as the field strength gets larger. In fact the linewidth will remain approximately constant in units of Hertz (about 150 Hz in this case) and will appear larger in units of ppm (normally used in all reported measurements) as the field is reduced. This means that the error bars on the lower field isotropic shift measurements will become larger and larger. This fact must be accounted for in the linear least squares analysis of the best fits (see figure 7.5). To do this, the contribution of each point to the least-squares chi-squared value must be weighted by the error in the measurement of that point. Figure 7.5 shows the plot of the measured isotropic shifts versus the reciprocal of the field strength squared. The best fits through each of the sets of isotropic shifts are shown.

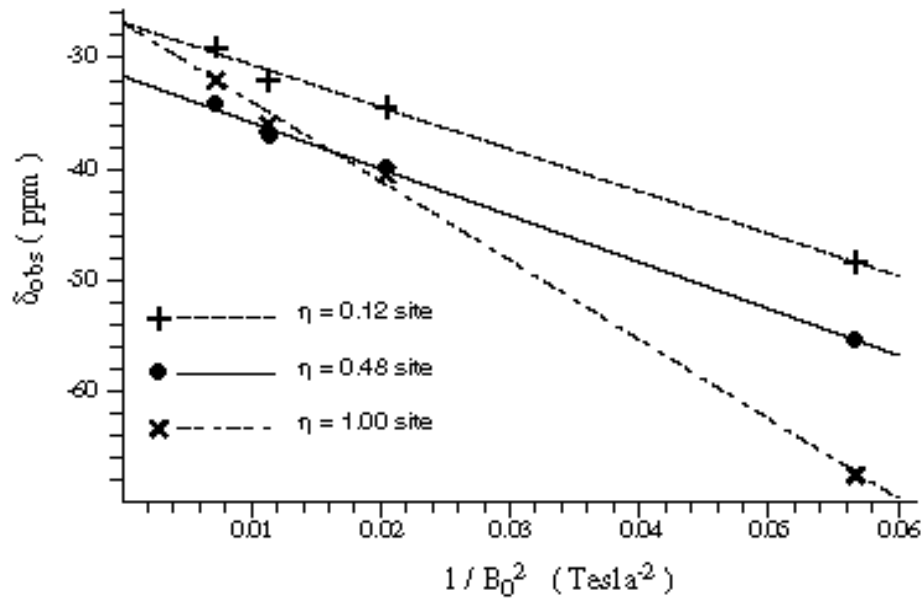


Figure 7.5 RbNO₃ Linear Regression of Isotropic Shifts versus $1/B_0^2$

This linear regression gives significant improvements in the overall errors. Figure 7.4 shows the DAS spectra at the four field strengths and Figure 7.5 shows the actual linear regression best fit. Table 7.3 gives the compiled final results and errors. As observed, the errors are about half as large as with only two fields (table 7.1). The isotropic shifts are all given in units of ppm and the quadrupolar coupling product is in units of MHz. In addition, when these results are compared to those from single site simulations (see next

section), the values for the quadrupolar and chemical shift parameters are much closer to the correct values.

$\delta_{obs}^{4.2T}$	$\delta_{obs}^{7.0T}$	$\delta_{obs}^{9.4T}$	$\delta_{obs}^{11.7T}$	$\delta_{iso}^{(CS)}$	P_Q
-48.4±3.0	-34.4±2.0	-32.0±1.0	-29.0±1.0	-26.8±0.8	1.72±0.06
-67.5±3.0	-39.8±2.0	-36.0±1.0	-32.0±1.0	-26.8±0.8	2.36±0.04
-55.3±3.0	-40.2±2.0	-37.0±1.0	-34.0±1.0	-31.6±0.8	1.81±0.05

Table 7.3 $^{87}\text{RbNO}_3$ Multiple Field DAS Results. Isotropic chemical shifts and quadrupolar products were calculated from a linear regression analysis of the isotropic shifts versus $1/B_0^2$ as in figure 7.6.

Improvements from MAS-Detected DAS

MAS detected DAS⁵⁰ was performed at both 9.4T and 11.7T (figures 7.6 and 7.7 respectively.) These spectra show a high resolution DAS dimension as well as a pure-phase MAS detected anisotropic dimension. Slices through each DAS peak yield accurate MAS lineshapes for each site. Figure 7.8 shows the simulation of each of the three sites and table 7.4 gives the most precise (because there is only one external standard) and accurate (essentially more data points are effectively involved in the calculation than in multiple field methods) $^{87}\text{RbNO}_3$ quadrupolar coupling and chemical shift parameters measured. In addition, by using both fields, even greater accuracy may be achieved by simulating both field spectra at the same time. This approach has been used previously for multiple site ^{17}O spectra⁴⁸ (see chapter 8). The pulse sequence used to collect these spectra is the double-hop DAS sequence described by Mueller *et al.*⁵⁰ This sequence achieves pure-absorption mode spectra by taking a hypercomplex data set in t_1 . The overall signal-to-noise ratio is greatly reduced as compared to the hypercomplex SEDAS experiment (by a factor of 8) due to the second z-filter storage period (used to store magnetization while we reorient the spinner between the second DAS angle to the magic-angle 54.74°) and the lack of an echo in the second dimension. However, in the case of

$^{87}\text{RbNO}_3$, the relaxation times and absolute signal intensity make collection of a MAS detected DAS spectrum quite feasible.

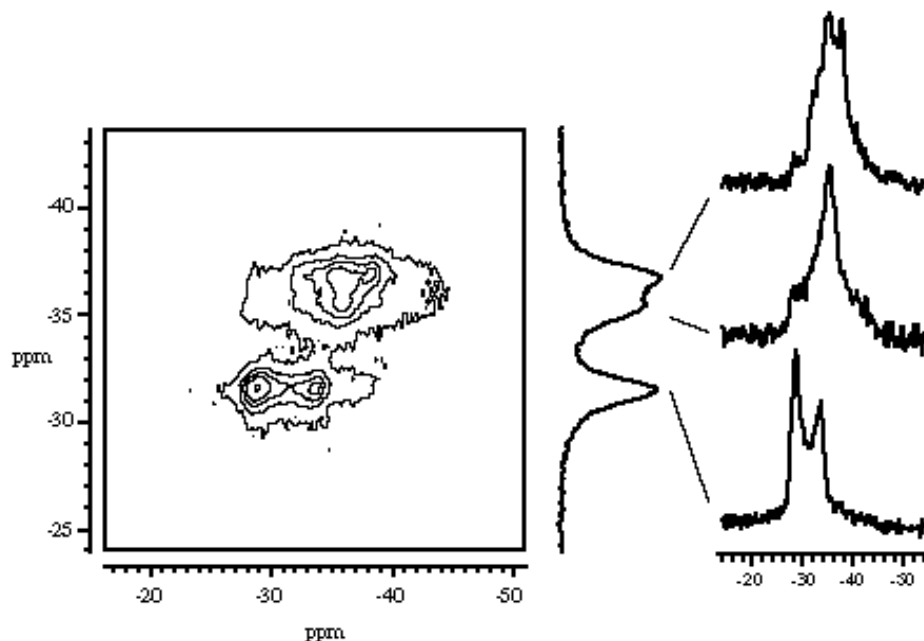


Figure 7.6 RbNO_3 9.4T 2D MAS detected DAS Contour Plot. Single site MAS slices through each isotropic peak in the DAS dimension have been extracted and are displayed to the right of the contour plot.

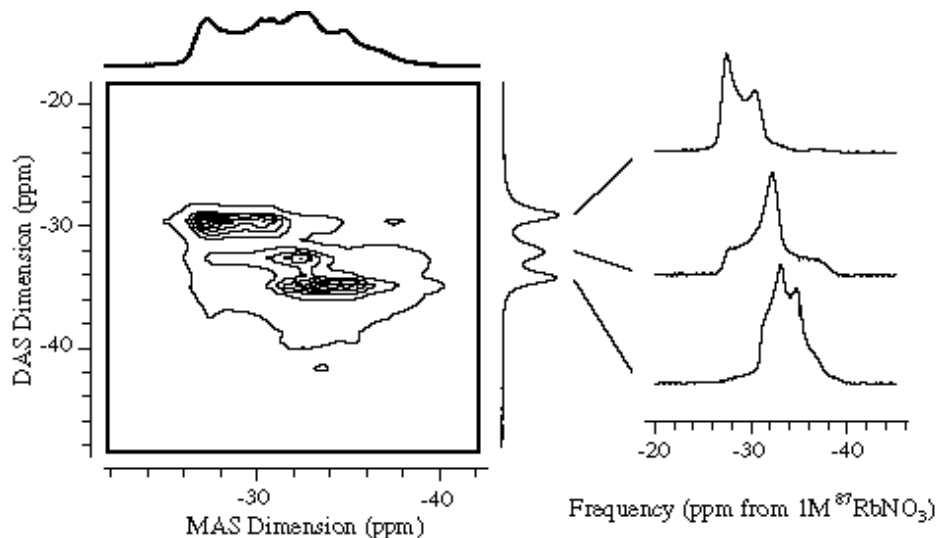


Figure 7.7 RbNO_3 11.7T 2D MAS detected DAS Contour Plot. Single site MAS slices through each isotropic peak in the DAS dimension have been pulled out and are displayed to the right of the contour plot.

In the 9.4T MAS detected DAS spectrum, figure 7.6, the site with a nearly zero asymmetry parameter at -32 ppm is clearly separated from the other two sites. The slice through

this peak may be fit easily with a single high speed MAS pattern. The other two sites overlap too much and the sum of the slices through these peaks must be simulated with two patterns. In the case of 11.7T MAS detected DAS, figure 7.7, all three sites are cleanly separated and may be simulated individually. Figure 7.8 shows each of the three slices through the isotropic DAS peaks at 11.7T, along with the best fit simulations. The parameters and error bars for these simulations are given in table 7.4 below.

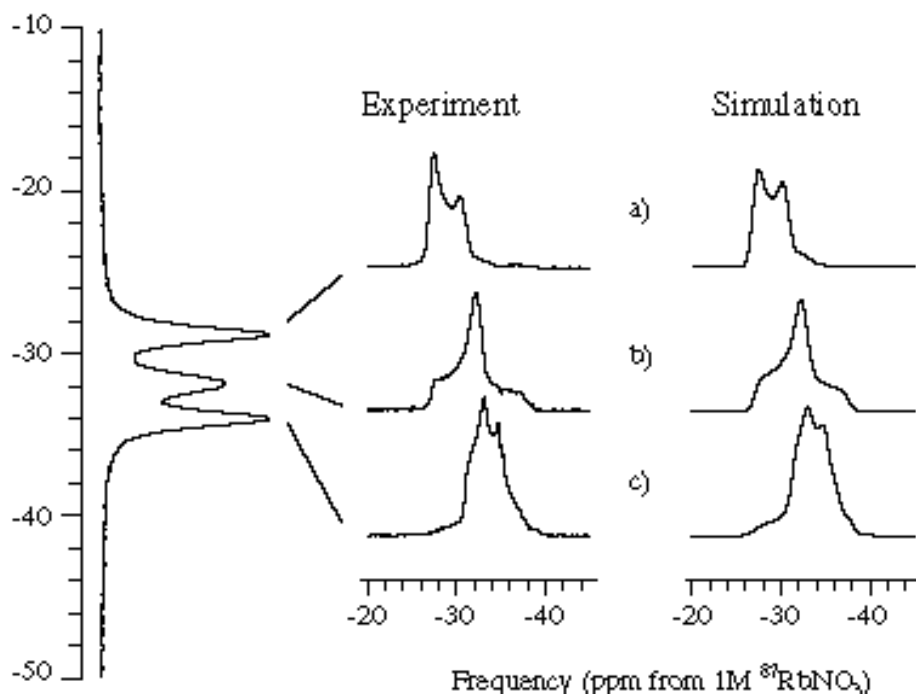


Figure 7.8 RbNO₃ Single Site MAS Slices and Simulations at 11.7T. Best fit parameters are given in table 7.3.

The isotropic shifts from these simulations agree quite well with the results from the four field linear regression fit of the isotropic shifts. The same type of simulation was performed on the ⁸⁷RbClO₄ MAS spectrum, yielding the results in table 7.4. The advantage with the MAS detected DAS method is that in this case, only a single field strength is needed with only a single experiment. The errors from this method are even less for the quadrupolar coupling constants than in the multiple field experiments of the previous section. The errors in the measurement of the isotropic chemical shifts, however, are larger since these are primarily systematic errors due to the external 1M ⁸⁷RbNO₃ fre-

quency reference. The combination of both the multiple field measurements and the MAS detected DAS experiments leads to the highest overall accuracy and precision in the determination of these parameters.

Compound	$^{(CS)}_{iso}$ (ppm)	C_Q (MHz)	
RbClO ₄	-16.2±1.0	3.20±0.05	0.10±0.05
RbNO ₃	-26.2±1.0	1.83±0.05	0.12±0.05
	-26.8±1.0	2.39±0.07	1.00±0.05
	-30.9±1.0	1.91±0.05	0.48±0.05

Table 7.4 ⁸⁷Rb Isotropic Shifts from MAS Simulations. The RbClO₄ values come from the simulation of the MAS spectrum (figure 7.2b) while the RbNO₃ values come from the simultaneous simulation of the 9.4T and 11.7T slices from figures 7.7 and 7.8.

Finally, the quadrupolar coupling constants for ⁸⁷RbNO₃ may be compared to those measured by Segel¹³⁶. In those low field measurements, he measured coupling constants of 1.76, 1.80 and 2.20 MHz and asymmetry parameters of 0.17, 0.48 and 0.91 for the three sites respectively. These are in very good agreement with the values measured with DAS experiments.

Theory of Coupling Constants from Crystal Structure

The RbNO₃ coupling constants also provide a good example to demonstrate how to use the measured quadrupolar information to assign resonances to actual sites in the crystal structure. To do this, we assign a point charge to each of the atoms in the RbNO₃ crystal structure. If for instance, we choose +1 for the rubidium atoms and -1/3 for each of the oxygen atoms, we may then calculate EFG tensor at each rubidium site. To do this, we use the unit cell centered at the origin and the 26 unit cells which directly surround the origin. The electric field gradients are calculated using the formula given below.

$$V(x_0, y_0, z_0) = \frac{-eq}{r} = \frac{-eq}{\sqrt{(x-x_0)^2 + (y-y_0)^2 + (z-z_0)^2}} \quad (7.4)$$

$$\frac{\partial^2 V(x_0, y_0, z_0)}{\partial \alpha \partial \beta} = V_{\alpha\beta} = \frac{eq}{r^5} (r^2 \delta(\alpha - \beta) - 3\alpha\beta)$$

Where α, β are coordinates x, y, z and $\delta(\alpha - \beta)$ is a Dirac delta function. With each electric field gradient (EFG) tensor element known, we may then diagonalize the tensor to get the principal axis values for V_{xx} , V_{yy} and V_{zz} . To convert these values into C_Q and η values, we need to use the relationships that relate V to quadrupolar coupling constants. In addition we need to know the Sternheimer anti-shielding factor. In the case of RbNO_3 we have calculated EFG values (see table 7.5) for a variety of point charge distributions. Changing the values of the charges changes the absolute size of the EFG tensor values, but does not appreciably change the asymmetry parameters. Therefore, we may assign each DAS peak to a site in the RbNO_3 crystal structure (unit cell not shown).

Rb Charge	N Charge	O Charge	Site	C_Q (a.u.)	
+0.70	-0.10	-0.20	1	3.5	0.31
			2	3.4	0.59
			3	3.5	0.97
+1.00	-0.10	-0.30	1	3.4	0.30
			2	3.4	0.61
			3	3.5	0.94
+0.60	+0.10	-0.23	1	3.4	0.29
			2	3.4	0.72
			3	3.5	0.81
+0.40	-0.10	-0.10	1	3.4	0.32
			2	3.4	0.55
			3	3.5	0.97

Table 7.5 $^{87}\text{RbNO}_3$ EFG Values From Crystal Structure. These calculations were carried out over a large number of unit cells and the EFG values were calculated and averaged for the thirty inner most Rb sites (out of almost 250 total).

Application of CPDAS to organic compounds

The use of solid state NMR to study biologically active and interesting compounds has been one of the longtime goals of many researchers. Techniques such as rotational resonance (R^2), spin echo double resonance (SEDOR), rotational echo double resonance (REDOR) and transferred echo double resonance (TEDOR) have been used successfully to measure distances at specific sites in a number of biological samples by research groups at MIT and Washington University.^{137,138} These techniques look primarily at the ^1H , ^{19}F , ^{13}C and ^{15}N nuclei in labeled compounds. The important oxygen nucleus has been studied much less. The primary reasons for this lack of ^{17}O information stems from its low gyromagnetic ratio (1/7 of ^1H), strong quadrupolar interactions and low natural abundance (0.037%). Isotopic substitution may be used to overcome the last problem and large magnetic fields may be used to fight the first (and to some degree the second). The strong second-order quadrupolar broadening in ^{17}O compounds is the largest obstacle remaining.

Recent developments in DAS have allowed us to begin to look more closely at ^{17}O . Specifically in the case of biological samples, decoupling of the ^1H nuclei is essential for high resolution. In addition, the long ^{17}O relaxation times and low sensitivity may be overcome with cross polarization techniques (as described in chapter 5). We have begun preliminary studies of L-alanine, one of the simplest amino acids which is present in virtually all proteins and peptides. The 20% enriched sample was made by H. Zimmerman by acid catalyzed exchange of oxygen in ^{17}O labeled water. The relaxation times in this compound are quite favorable for DAS, with a 700 ms ^1H relaxation time (this determines the experimental repetition rate) and 2.5 s for the ^{17}O (which determines the minimum rotor reorientation time).

For the cross polarization experiments on ^{17}O labeled L-alanine at 7.04 T the 3/4" static coil DAS probe designed by Mueller *et al.*⁵¹ was refitted with a double tuned ^1H - ^{17}O rf circuit capable of absorbing 500 W decoupling pulses on the ^1H channel (301.2

MHz). The circuit used is a standard one described previously by Doty *et al.*^{139,140} The ^1H and ^{17}O central transition selective pulses were both approximately $7\ \mu\text{s}$. The dwell times were $12.5\ \mu\text{s}$ in the t_2 dimension and $18\ \mu\text{s}$ in the t_1 dimension (after shearing). The angle pair was the usual $0^\circ\text{-}63.43^\circ$ ($k = 5$) to obtain maximum CP efficiency.

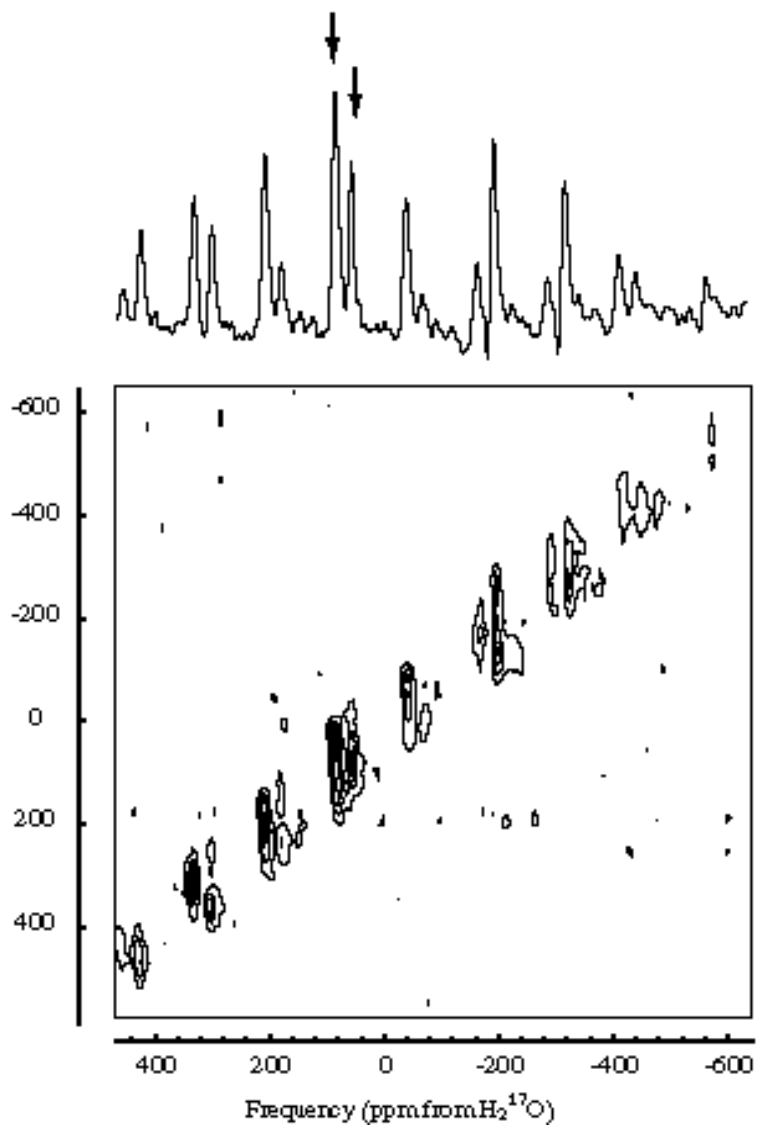


Figure 7.9 ^1H Decoupled Two-Dimensional ^{17}O CPDAS Spectrum of Alanine at 7.0T. The experimental parameters are given in the text. The two isotropic peaks are labeled with arrows. All other peaks in the DAS dimension are spinning sidebands.

The spinning rate was 6 kHz and the hopping time was 35 ms. In these experiments, 256 points were taken in the anisotropic dimension and 117 in the isotropic DAS dimension. The data in figure 7.9 was zero-filled to 256×256 for final processing. L-Alanine has

two crystallographically distinct oxygen sites in the unit cell¹⁴¹. The two isotropic peaks for the distinct oxygen sites in L-alanine were observed at 51 ± 4 and 80 ± 4 ppm from the ^{17}O labeled water standard. All other peaks in the spectrum in figure 7.9 are spinning sidebands.

The spectra of alanine taken at 11.7T used a standard single tuned probe.⁵¹ At this high (500 MHz) proton frequency, no decoupling could be achieved and the oxygen lines are significantly broader (almost a factor of 10) than in the decoupled spectrum at 7.04T.

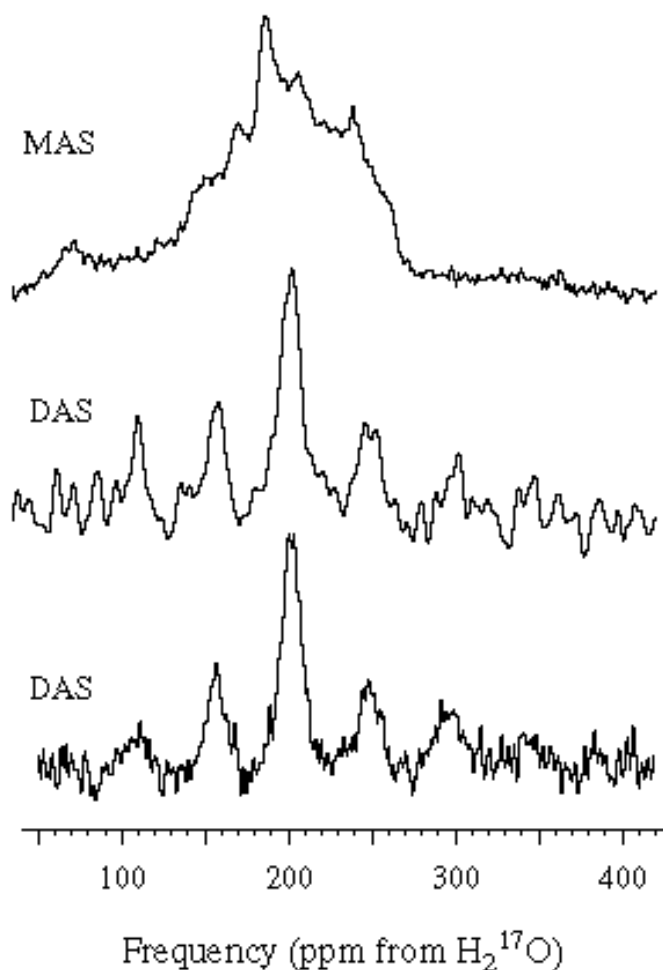


Figure 7.10 Undecoupled ^{17}O MAS and DAS Spectra of Alanine at 11.7T. The experimental parameters for these experiments are given in the text. The isotropic peak in the DAS spectrum occurs at 200 ppm; all other peaks are spinning sidebands.

The $\pi/2$ selective pulses were again $7.0 \mu\text{s}$; most other parameters were similar to those used at 7.04 T. Figure 7.10 shows both the MAS and two DAS spectra for the same alanine sample as in figure 7.9. The MAS spectrum shows a broad powder pattern with a number of singularities. The two peaks in the DAS spectrum are not clearly resolved and are both assigned an isotropic shift of 200 ± 7 ppm. Using the two field results (just as in the case of the ^{87}Rb salts of the previous section) we may calculate the isotropic chemical shifts and quadrupolar coupling products for the two sites in alanine. These results are compiled in table 7.6 below.

Site	$\delta_{obs}^{7.04T}$	$\delta_{obs}^{11.7T}$	P_Q (MHz)	δ_{isacs}
1	51 ± 4 ppm	200 ± 7 ppm	8.1 ± 0.3 MHz	285 ± 8 ppm
2	80 ± 4	200 ± 7	7.2 ± 0.3	268 ± 8

Table 7.6 ^{17}O L-Alanine DAS Results. Multiple field measurements from figures 7.9 and 7.10 are tabulated along with the calculated quadrupolar products and isotropic chemical shifts. The error bars are indicated and arise from the overall width of the peaks in the DAS spectra.

These values for the quadrupolar coupling products are in good agreement with the size of the quadrupolar coupling constant measured for the carboxyl oxygen atoms in similar compounds with NQR. Additional experiments are currently underway which will apply the techniques of CPDAS and DAS to other organic compounds with the long term goal of examining larger biologically active molecules.